

pubs.acs.org/NanoLett Letter

Quantum Spin Hall Edge States and Interlayer Coupling in Twisted Bilayer WTe₂

Felix Lüpke,* Dacen Waters, Anh D. Pham, Jiaqiang Yan, David G. Mandrus, Panchapakesan Ganesh, and Benjamin M. Hunt



Cite This: Nano Lett. 2022, 22, 5674-5680



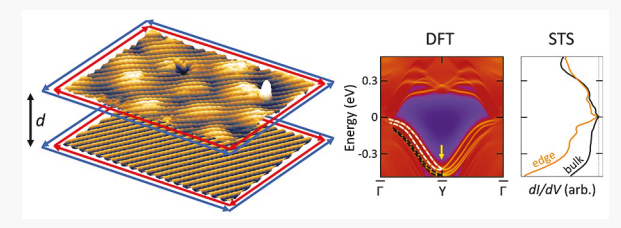
ACCESS

Metrics & More

Article Recommendations

Supporting Information

ABSTRACT: The quantum spin Hall (QSH) effect, characterized by topologically protected spin-polarized edge states, was recently demonstrated in monolayers of the transition metal dichalcogenide (TMD) WTe₂. However, the robustness of this topological protection remains largely unexplored in van der Waals heterostructures containing one or more layers of a QSH insulator. In this work, we use scanning tunneling microscopy and spectroscopy (STM/STS) to explore the topological nature of twisted bilayer (tBL) WTe₂. At the tBL edges, we



observe the characteristic spectroscopic signatures of the QSH edge states. For small twist angles, a rectangular moiré pattern develops, which results in local modifications of the band structure. Using first-principles calculations, we quantify the interactions in $tBL\ WTe_2$ and its topological edge states as a function of interlayer distance and conclude that it is possible to engineer the topology of WTe_2 bilayers via the twist angle as well as interlayer interactions.

KEYWORDS: Topological insulators, van der Waals heterostructure, twisted bilayers, scanning tunneling microscopy, quantum spin Hall edge states

he variety of layered two-dimensional (2D) materials available for isolation and fabrication into van der Waals heterostructures provides almost endless combinations for device engineering. 1T'-TMDs have attracted recent attention among the layered materials following the prediction of the QSH edge state in the monolayer (ML) limit.² In particular, WTe2 has been of great interest due to its realization of multiple exotic physical phenomena depending on its thickness. Monolayer 1T'-WTe2 has been reported to exhibit the predicted QSH effect, which persists up to 100 K3-6 and further hosts a superconducting phase below ~1 K, when electrostatically gated into the conduction band.^{7,8} Bilayer (BL) WTe₂ on the other hand is predicted to be a topologically trivial semimetal, which has also been shown to exhibit ferroelectric switching when a surface normal electric field is applied. 10 In the bulk limit, WTe2 was reported to realize a type-II Weyl semimetal and higher-order topological phase with 1D hinge states. 11,12 The high degree of layer tunability in WTe2 makes it an attractive candidate for integration in van der Waals heterostructures, e.g., to realize one-dimensional topological superconductivity. 13 However, there are open questions, such as the effect of coupling to neighboring layers on the topological properties, which have to be thoroughly understood for applications of the topological edge states in electronic devices.

Recently, the interactions between rotationally misaligned layers of 2D materials have attracted attention as hosts of a variety of interesting highly correlated phenomena such as

insulating states, superconductivity, and unique topological phases. 14-19 While most studies of twisted bilayers seek to achieve highly correlated states through a moiré pattern, in which flat bands emerge in the electronic structure, 14,15,17,19-22 here we focus on the effects of interlayer coupling on the already present QSH edge state in ML WTe2. We find that for incommensurately stacked twisted bilayer WTe2, both layers retain their topology, which results in two sets of QSH edge states sitting on top of each other. We experimentally study the edge states and interlayer coupling for multiple twist angles and rationalize our results based on first-principles calculations, demonstrating the robust topological protection of the QSH edge state predicted in the literature.²³ In contrast to twisted bilayers, we do not observe an edge state feature at the topologically trivial natural bilayer WTe2 edge. The topologically trivial nature of bilayer WTe2 is supported by our observation of a QSH edge state in monolayer WTe2 at a monolayer-bilayer junction.

To explore the QSH edge state in exfoliated WTe₂, we study WTe₂/MoS₂ heterostructures (Figure 1a). Samples are fabricated using a recently developed dry transfer flip

Received: February 1, 2022 Revised: June 7, 2022 Published: June 27, 2022





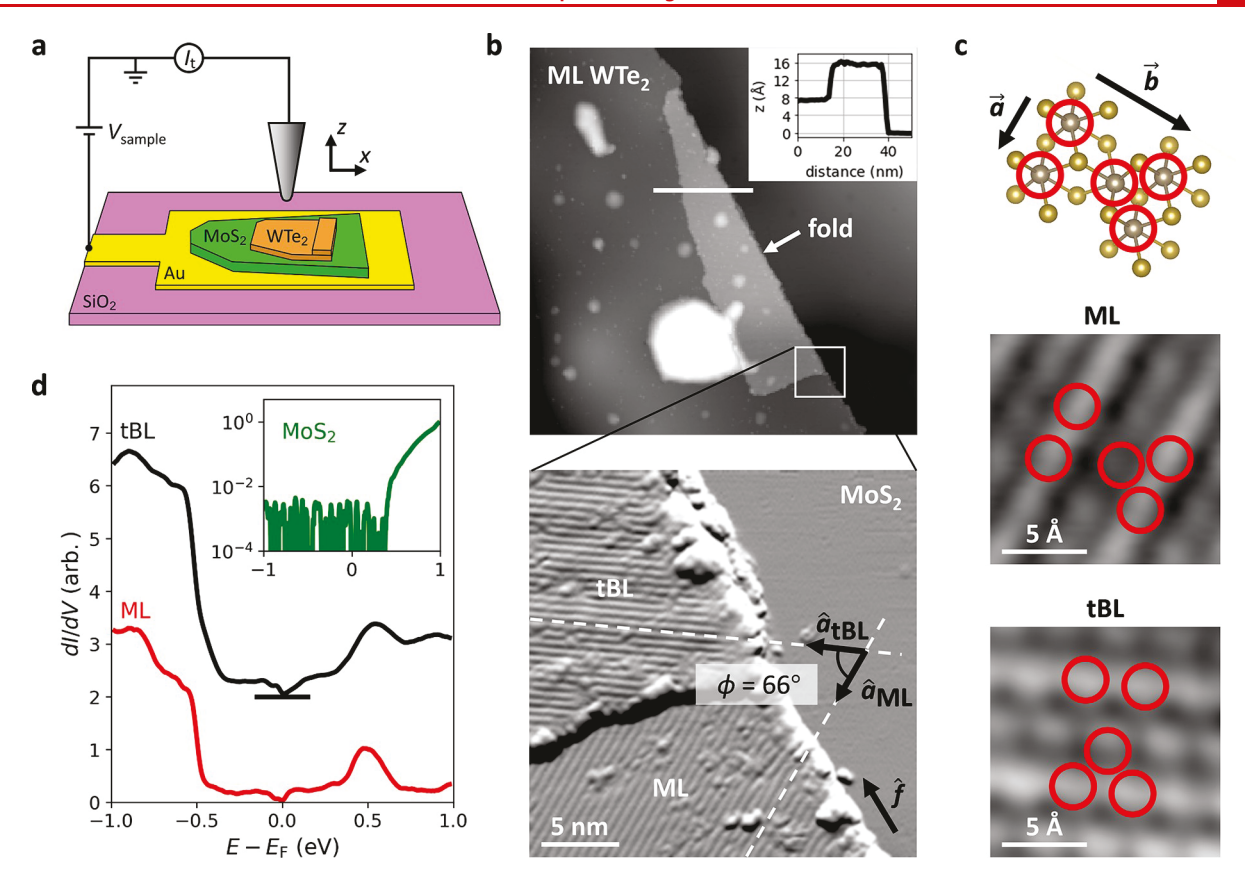


Figure 1. Twisted bilayer WTe₂/MoS₂ heterostructure. (a) Schematic of the tunneling experiment. (b) Large area scan (200 nm) of a WTe₂ monolayer with a folded edge on a MoS₂ substrate flake. Inset: Height profile across the folded WTe₂ bilayer showing layer thicknesses corresponding to single-layer step heights of WTe₂, indicating atomically clean interfaces. The relative rotational misalignment of the WTe₂ atomic rows in the two regions is evident in the detail image (gradient image shown), realizing a WTe₂ twisted bilayer (tBL). The fold axis \hat{f} is parallel to the resulting WTe₂–MoS₂ step edge. (c) Atomic model of the WTe₂ unit cell and atomically resolved images, from which we determine the lattice misorientation between the two WTe₂ layers to be $\phi = 66^{\circ}$ (tunneling parameters $V_{\text{sample}} = -0.4 \text{ V}$, $I_{\text{t}} = 20 \text{ pA}$). Red circles mark the positions of the W atoms with $|\vec{a}| = 3.48 \text{ Å}$ and $|\vec{b}| = 6.28 \text{ Å}$. (d) Tunneling spectroscopy on the two WTe₂ regions reveals almost identical electronic structures, while the MoS₂ substrate flake shows a band gap around the Fermi energy with the conduction band edge located at ~0.5 eV.

technique that allows the stacking of van der Waals materials while maintaining atomically clean surfaces and interfaces (for details see Materials and Methods, section S1 and ref 13). MoS₂ is used as a substrate flake to provide an atomically flat support for the WTe₂. The typical signature of the WTe₂ QSH edge state in the energy range ($-0.5 \lesssim V_{\rm sample} \lesssim 0$ V) is located in the MoS₂ band gap so that substrate effects can be excluded when analyzing the edge state spectra. In addition, we can tunnel into the MoS₂ conduction band at a sample bias of $V_{\rm sample} \gtrsim 0.5$ V, allowing us to safely scan over the edge of the WTe₂ flakes.

In large area scans of the heterostructures, we find random folds along the edge of the WTe₂ monolayer (Figure 1b). Such folds occur by accident during the exfoliation and dry transfer and are usually undesired, e.g., for fabrication of transport devices. However, the fold offers a unique opportunity to study the interaction between the QSH edge states, which are naturally located right on top of one another along the fold. A profile across the folded region shows a ML step height of \sim 7.5 Å, i.e., slightly larger than for WTe₂ monolayers on graphene or NbSe₂, ^{4,13} which we attribute to the electronic contrast between the respective substrate materials and the WTe₂. The step height from the first to the second WTe₂ layers is also \sim 7.5 Å, which slightly deviates from the natural bilayer step height (\sim 7.1 Å^{13,24}). This deviation can be explained by the

incommensurate stacking of the rotationally misaligned layers, resulting in a larger interlayer separation. The sharpness of the tBL step edge indicates that it is no longer connected to the layer below and must have been separated during fabrication as a result of the fold. Owing to the in-plane screw axis of the 1T' monolayer, a folded bilayer is entirely equivalent to two stacked monolayers with a twist angle ϕ determined by the fold axis (see section S2). Defect-free atomic resolution images of the ML and folded bilayer (Figure 1c) resemble pristine WTe₂ reported in the literature. ^{4,24} From the orientation of the atomic resolution images, we determine the relative twist angle t h e between t w o layers t o $\phi = |\cos^{-1}(\hat{a}_{\text{ML}} \cdot \hat{a}_{\text{tBL}})| = 66^{\circ} = |2 \cos^{-1}(\hat{f} \cdot \hat{a}_{\text{ML}})|, \text{ where } \hat{f} \text{ is}$ the fold axis orientation. For reference, natural bilayer WTe2 corresponds to $\phi = 180^{\circ}$ by this definition. As a result of the large twist angle, we do not observe a pronounced moiré pattern, and spectra taken on the folded region are almost identical to those of monolayer WTe2, indicating decoupled layers (Figure 1d). This observation implies that there should be two independent sets of QSH edge states, one in each layer, which we explore in the following.

First, we examine the ML WTe₂ edge (Figure 2a), where we find the typical spectroscopic signature of the QSH edge state, in the form of an enhanced density of states below $E_{\rm F}$, in agreement with the literature.^{4,13,24} The QSH edge state is

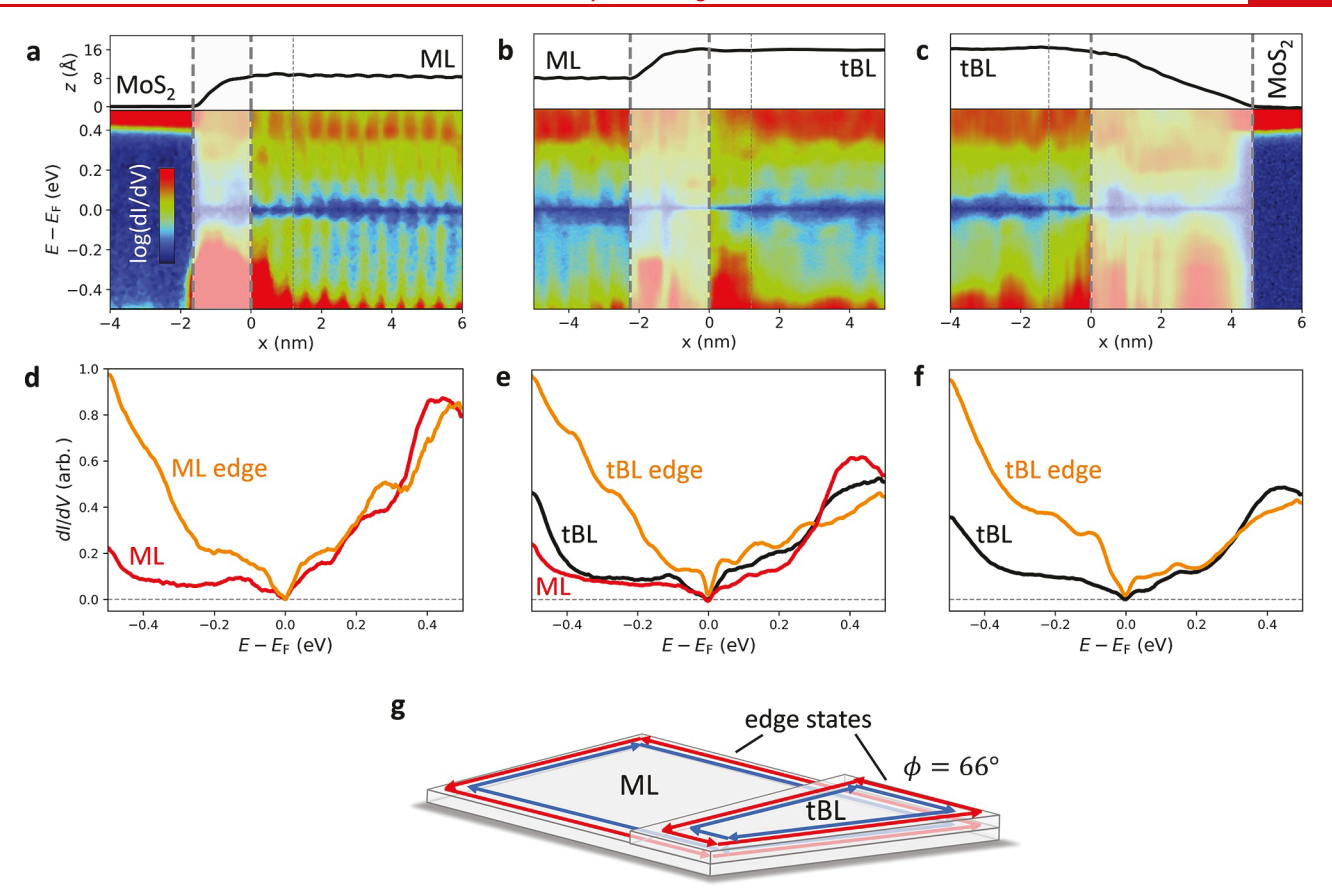


Figure 2. Observation of edge states in twisted bilayer WTe₂. (a) Tunneling conductance across the ML WTe₂ step edge. The location of the topographic edge (x = 0 nm) is extracted using a systematic edge detection scheme (see text). Right of the edge, the flat terrace of the WTe₂ monolayer is measured. Here, the QSH edge state consistently appears as an enhanced density of states below the Fermi energy and decays into the monolayer. The decay length is in agreement with the literature value of ~1.2 nm (indicated by a dotted line). In the region to the left of the edge, between $-1.5 \lesssim x \leq 0$ nm, the topography deviates from the flat terrace, and the measured signal can be affected by edge reconstructions and artifacts due to the finite size of the STM tip. This "transition region" (indicated by dashed lines and overlaid in gray) is therefore excluded from the analysis. (b) Tunneling conductance across the ML-tBL step edge showing the presence of an edge state on top of the tBL terrace. Dashed and dotted lines defined as in (a). (c) Tunneling conductance across the tBL-MoS₂ step edge similarly showing the presence of an edge state on the tBL. (d-f) Tunneling spectra extracted from (a-c), averaged over the spatial extent of the indicated edge state regions and far away from the edges, respectively. The *y*-axis scale is identical for (d-f). (g) Schematic of the topological edge states in a rotationally misaligned WTe₂ homobilayer, reflecting our observations.

observed on the flat terrace next to the onset of the topographic step edge, which distinguishes it from edge effects, such as edge reconstructions, and tip artifacts that can occur in the transition region due to the finite tip size. We systematically identify the positions of the topographic edges—namely, x=0 nm, and the extension of the transition regions in Figures 2a–c and 3c,d—as the points where the topography gradient reaches a threshold value of $dz/dx=\pm 1.5$ Å/nm (see section S6 for details). Using this detection scheme, we find that the spatial extent of the QSH edge state on the ML WTe₂ terrace is ~1.2 nm, in agreement with that observed in WTe₂ on graphene⁴ and on NbSe₂¹³ and similar to what has been predicted theoretically.²⁵

Turning now to the $\overline{\text{ML-tBL}}$ edge, we observe a similarly enhanced density of states, which again extends ~1.2 nm from the step edge (Figure 2b), indicating the presence of an edge state in the upper $\overline{\text{WTe}}_2$ layer, since STM is sensitive almost exclusively to the topmost layer. Furthermore, we observe the same increase in density of states at the edge along the fold, where the tBL steps down to the $\overline{\text{MoS}}_2$ (Figure 2c), again with the same lateral extent. Along this edge, the two sets of QSH edge states sit on top of each other, which is in contrast to

interior edges, for which the QSH edge states can only interact with the (gapped) underlying bulk. Comparing individual spectra extracted from the conductance maps (Figure 2d-f), it is evident that the spectra far away from the edge of the ML WTe2 and the tBL WTe2 are very similar over this energy range. In addition, the spectra at the edges of the ML and tBL WTe2 all show a very similar enhanced density of states below $E_{\rm F}$, which is consistent with the typical signature of the QSH edge state. We conclude that the individual layers are decoupled, each with their own QSH edge state (Figure 2g). In principle, backscattering between the QSH edge states of the two layers is suppressed only for small twist angles, due to the canted edge state spin-axis and monolayer screw symmetry.26 However, as a result of the weak interlayer coupling, we expect that interlayer scattering from the edge state of one layer into the edge state of the other layer is negligible for larger twist angles as well. In combination with the prohibited intralayer backscattering, this suggests a strong protection of the QSH edge states at the folded tBL WTe₂ edge (see also Figure S6). We support this finding by studying a second folded region, which has two domains, allowing the

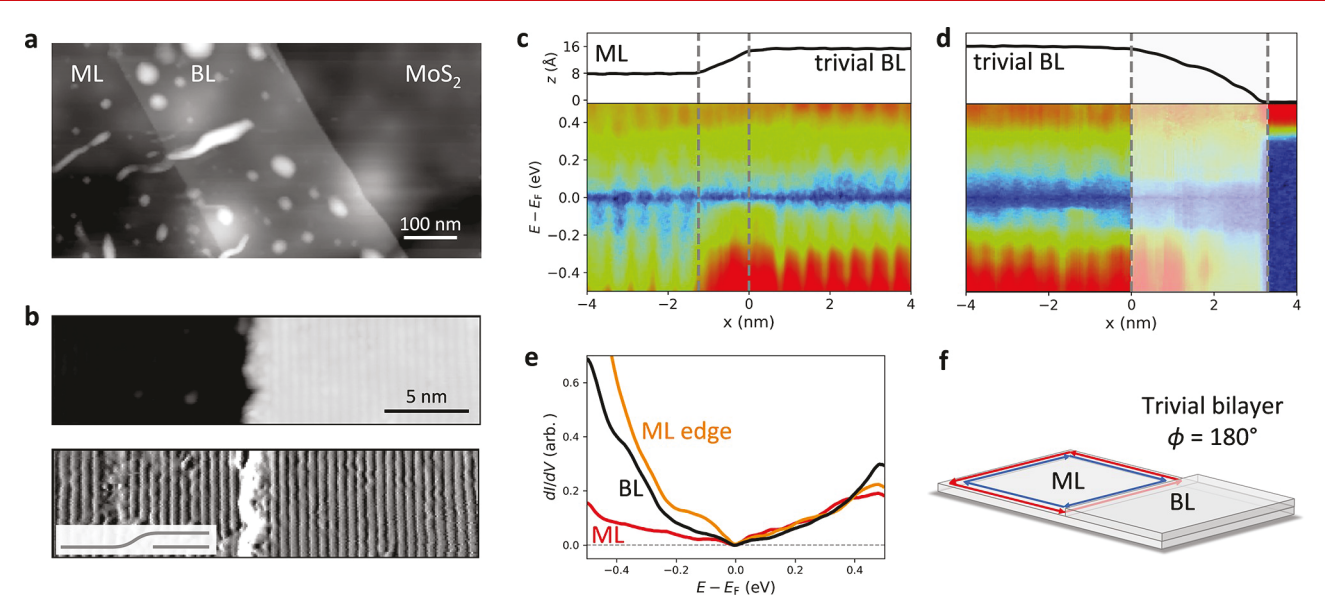


Figure 3. Edge state at a monolayer/natural bilayer junction. (a) Large area scan of an exfoliated natural WTe₂ bilayer connected to a monolayer. (b) Atomic resolution scan and gradient of the ML-BL junction showing parallel atomic rows. The top layer is expected to be continuous as a result of the sample fabrication technique and therefore can be measured free from significant tip artifacts (inset: schematic of the top layer draped over the second layer underneath). (c,d) Tunneling conductance measured across the ML-BL edge and BL-MoS₂ edge, showing no signature of an edge state on the BL terrace. However, we observe an increase in the density of states in the transition region between the ML and BL, which is identical to the signature of the QSH state shown in Figure 2a. (e) Tunneling spectra extracted from (c) and (d), averaged over the spatial extent of the indicated edge state region and far away from the edges, respectively. (f) Schematic of the QSH edge state in a WTe₂ ML-BL junction.

characterization of two additional twist angles as well as the lateral domain boundary state (see sections S4 and S5).

Next, we explore a step edge between a WTe2 monolayer and a topologically trivial natural bilayer (Figure 3a,b). In the present sample, the top WTe2 layer of the natural bilayer is continuous and draped over the second layer underneath due to the flipping of the sample during fabrication. With multiple iterations of very carefully prepared sharp tips, we are able to resolve the draped monolayer free from significant tip artifacts and measure the tunneling conductance across the ML-BL junction (Figure 3c and section S7). We find that there is a clear increase in the density of states in the WTe2 monolayer just before the bilayer, again with an extension of \sim 1.2 nm. The shape of this feature (Figure 3c) shows remarkable agreement to that observed at the monolayer WTe₂/MoS₂ edge in Figure 2d. We therefore conclude that the spectroscopic feature at the ML-BL junction is the manifestation of the QSH edge state between the topological WTe2 monolayer and the topologically trivial natural WTe2 bilayer (Figure 3f). This finding verifies that there is a significant interlayer interaction in aligned, natural bilayer WTe2, which is in contrast to the above studied twisted bilayers. Such an interlayer-interaction-induced change in topology between the monolayer and bilayer is in agreement with WTe2 undergoing another topological transition at higher layer number, possibly to a higher-order topological phase. 12 The corresponding edge states of bulk WTe2 have an electronic structure²⁷ that is distinctly different from the edge states observed in ML and tBL WTe2, indicating that these are in fact different topological states.

In order to analyze the effect of interlayer interactions in greater detail, we further study a tBL sample, which we fabricate using a modified tear-and-stack technique (for details see Materials and Methods and section S8). The tear-and-stack sample fabrication allows us to directly control the twist angle

and therefore manifest a moiré pattern, in which the interlayer coupling is expected to be modulated across the moiré unit cell. The resulting long-range moiré pattern has a rectangular unit cell and periodicity of \sim 6.5 nm (Figure 4a,b). The corresponding twist angle is $\phi \approx 5.5^{\circ}$ following the same angle definition as with the folded bilayer, which we also directly confirm at the tBL edge (Figure S11). Resulting from the different stacking of W atoms, we observe two different corrugation maxima in the moiré unit cell, where the A-site W atom in one layer vertically aligns with the A- or B-site W atom of the other layer, i.e., AA- or AB-stacking, respectively. Due to the rectangular shape of the moiré unit cell, the AA-stacked sites form a distinct quasi-one-dimensional pattern, which has been proposed to result in an array of 1D Luttinger liquids at low energy. Second Sec

Tunneling spectra recorded in different positions of the moiré unit cell (Figure 4c) show distinctly different spectral features. In AA-stacked positions, the conduction band peak at 0.5 eV shows a significant splitting, while spectra taken in AB sites show a stronger hybridization in the valence bands when compared to ML WTe2. Spectra taken at C-stacked locations, where the unit cells are shifted by $\sim \vec{b}/2$ with respect to each other, show similarity to those of the natural bilayer, with a valence band feature at ~ -0.3 eV. Interestingly, this observation roughly coincides with the arrangement of W atoms in this location of the tBL moiré unit cell being similar to that of the natural bilayer, despite the C-stacked WTe₂ having a $\sim 0^{\circ}$ twist compared to the natural bilayer's 180° (see section S8 and Figure S12). Since the topography at this position is close to a minimum in the topography, we expect the layer hybridization to be stronger than in AA- and ABstacked regions. In combination, we attribute the distinct changes of the local electronic structure to the different interlayer interactions, which are the result of the local stacking geometry.

Nano Letters pubs.acs.org/NanoLett Lette

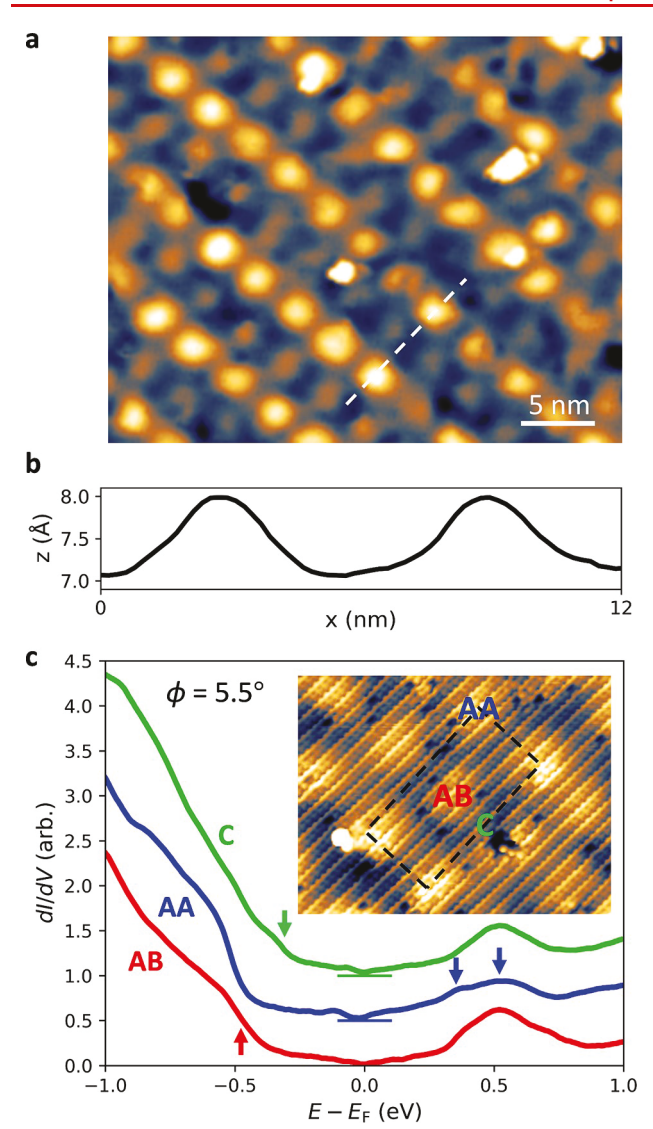


Figure 4. Tear-and-stack twisted bilayer WTe₂. (a) Large scale topography of the moiré pattern with periodicity corresponding to $\phi = 5.5^{\circ}$ ($V_{\rm sample} = -2$ V, $I_{\rm t} = 20$ pA). (b) Height profile of the moiré pattern along the dashed line in (a). (c) Tunneling conductance in different regions of the moiré unit cell. While at the AA-stacked site the conduction band peak is split (blue arrows), at the AB-stacked site, the valence band edge is broadened (red arrow), demonstrating distinct electronic properties within the moiré unit cell. Spectra taken at C-stacked sites show an increase in the valence band intensity at $E - E_{\rm F} = -0.3$ eV (green arrow), which results in a spectrum similar to that of natural BL shown in Figure 3e. Inset: Atomic resolution topography with the moiré unit cell indicated in white ($V_{\rm sample} = -1$ V, $I_{\rm t} = 55$ pA).

To understand the influence of interlayer distance and stacking on the electronic and topological properties of the WTe₂ bilayers, we performed density functional theory (DFT) calculations of a WTe₂ monolayer, natural bilayer ($\phi = 180^{\circ}$), as well as a bilayer with $\phi = 0^{\circ}$, most closely resembling our experiments on small twist angle tBLs. Details of the calculated band structures are found in the Materials and Methods and the Supporting Information. In general, we find that weakly coupled WTe₂ bilayers can be regarded as two decoupled monolayers, each retaining the electronic character of a WTe₂ monolayer, i.e., the QSH state ($\mathbb{Z}_2 = 1$). When bringing the layers closer together, they begin to interact and hybridize,

leading to a global trivial topology, $\mathbb{Z}_2 = 0$, in agreement with our experiments and earlier studies. The resulting charge transfer between the layers further leads to an increasing shift of their edge states with respect to each other (Figure 5). We

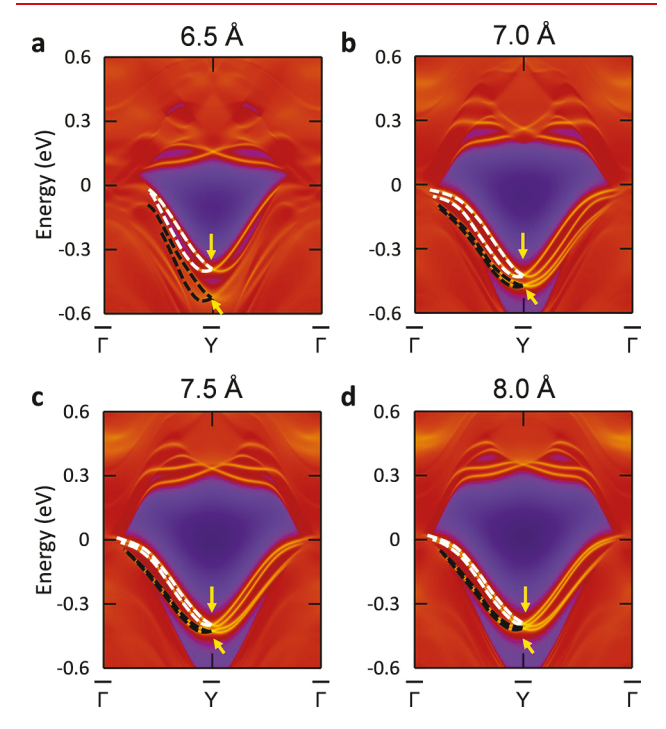


Figure 5. Dependence of tear-and-stack bilayer edge states on interlayer spacing. (a–d) Calculated band structures of a $\phi=0^\circ$ T' bilayer at interlayer distances of d=6.5 Å to d=8.0 Å. As the layers are moved further apart from each other, their QSH edge states become increasingly closer in energy due to a reducing charge transfer between the layers. When the layers are completely decoupled, the edge states are identical to that of WTe₂ ML. Black and white dashed lines in the left half of each panel indicate the edge state spin orientation in each of the two layers, respectively. Arrows indicate the respective Dirac points.

further investigate the effect of the subtle structural differences between the 1T' and the 1T_d phase on our calculations (see section S9) and find that the electronic and topological properties are strongly dependent on the stacking geometry owing to their different symmetries and interlayer spacings, which result in different amounts of charge transfer between the layers (Figures S21 and S22). Interestingly, as we bring the bilayers very close together ($d \approx 7.25$ Å in AA stacking), our calculations predict another topological transition back to $\mathbb{Z}_2 = 1$ for the T_d phase (section S9 and Figure S17). This interlayer distance is however significantly smaller than the $d \approx 8$ Å realized in the AA location of our $\phi = 5.5^{\circ}$ sample.

In summary, we report the presence of characteristic edge states in tBL WTe_2 for a total of four different twist angles, including along a coinciding edge where two sets of QSH edge states sit on top of the other as well as a lateral domain boundary. By comparison to experimental results at the boundaries of natural bilayer WTe_2 as well as DFT calculations, we conclude that it is possible to engineer the topology of WTe_2 bilayers via their twist angle and interlayer interactions.

Nano Letters pubs.acs.org/NanoLett Letter

MATERIALS AND METHODS

Sample Preparation. WTe₂ and MoS₂ were exfoliated onto 285 nm SiO₂/Si substrates. Exfoliating WTe₂ crystals produces flakes that have a high probability of producing edges that are aligned with one of the two crystal axes. We picked up a (20 ± 1) nm-thick MoS₂ flake with a PPC/PDMS stamp and subsequently a WTe2 flake containing mono- and bilayer regions. After the WTe2 pickup, the heterostructure was flipped upside down and placed onto a gold lead on an SiO₂ substrate, which was premounted and contacted to an STM sample plate. The tear-and-stack sample was fabricated in the same way, except that two pick-ups of the WTe2 took place with a slight rotation of the substrate after the first pickup. The exfoliation and stacking took place in a nitrogen-filled glovebox, from which the samples were transferred into a high vacuum tube furnace to remove the PPC by annealing at 250 °C for 8 h. Subsequently, the samples are transferred into the STM ultrahigh vacuum chamber where a final anneal at 250 °C for ~10 min ($p \le 1 \times 10^{-8}$ mbar) was performed; all sample transfers took place in nitrogen atmosphere.

STM Measurements. STM measurements are performed using a commercial CreaTec setup with a sample stage temperature of 4.7 K. Electrochemically etched tungsten tips were indented and checked for a clean spectrum on the gold leads prior to and in between measurements. The measurements throughout the manuscript have been performed with multiple iterations of freshly prepared tip apexes to exclude tip artifacts. dI/dV measurements were performed using a lock-in amplifier set to a frequency of f=869 Hz, at stabilization set point $V_{\rm sample}=500$ mV, $I_{\rm t}=50$ pA, and a modulation amplitude $V_{\rm mod}=10$ mV, except for Figures 1d and 4c, for which we used $V_{\rm sample}=1$ V, $I_{\rm t}=100$ pA, and a modulation amplitude $V_{\rm mod}=20$ mV.

DFT Calculations. Calculated band structures show the density of states in k-space (color coded), as a function of k_y and binding energy with respect to $E_{\rm F}$. Details of the DFT calculations can be found in the Supporting Information.

ASSOCIATED CONTENT

Supporting Information

The Supporting Information is available free of charge at https://pubs.acs.org/doi/10.1021/acs.nanolett.2c00432.

- (1) Details of the sample fabrication and experiments.
- (2) Additional discussion of crystal symmetries. (3) Additional experimental data of further twist angles and the topologically trivial domain boundary state. (4) Details of the DFT calculations and additional theoretical results (PDF)

AUTHOR INFORMATION

Corresponding Author

Felix Lüpke — Department of Physics, Carnegie Mellon University, Pittsburgh, Pennsylvania 15213, United States; Center for Nanophase Materials Sciences, Oak Ridge National Laboratory, Oak Ridge, Tennessee 37831, United States; Department of Materials Science and Engineering, University of Tennessee, Knoxville, Tennessee 37996, United States; Peter Grünberg Institut (PGI-3), Forschungszentrum Jülich, 52425 Jülich, Germany; orcid.org/0000-0002-6430-9627; Email: f luepke@fz-juelich.de

Authors

Dacen Waters — Department of Physics, Carnegie Mellon University, Pittsburgh, Pennsylvania 15213, United States; Department of Physics, University of Washington, Seattle, Washington 98195, United States; ◎ orcid.org/0000-0003-3588-0039

Anh D. Pham – Center for Nanophase Materials Sciences, Oak Ridge National Laboratory, Oak Ridge, Tennessee 37831, United States

Jiaqiang Yan — Materials Science and Technology Division, Oak Ridge National Laboratory, Oak Ridge, Tennessee 37831, United States

David G. Mandrus — Department of Materials Science and Engineering, University of Tennessee, Knoxville, Tennessee 37996, United States; Materials Science and Technology Division, Oak Ridge National Laboratory, Oak Ridge, Tennessee 37831, United States; Department of Physics and Astronomy, University of Tennessee, Knoxville, Tennessee 37996, United States; orcid.org/0000-0003-3616-7104

Panchapakesan Ganesh — Center for Nanophase Materials Sciences, Oak Ridge National Laboratory, Oak Ridge, Tennessee 37831, United States; orcid.org/0000-0002-7170-2902

Benjamin M. Hunt – Department of Physics, Carnegie Mellon University, Pittsburgh, Pennsylvania 15213, United States

Complete contact information is available at: https://pubs.acs.org/10.1021/acs.nanolett.2c00432

Author Contributions

F.L. and D.W. fabricated the samples, measured and analyzed the experimental data, and wrote the manuscript. P.G. and A.D.P. performed the DFT calculations, interpreted the results, and contributed to writing the manuscript. J.Y. and D.G.M. grew the WTe₂ crystals. B.M.H. supervised the project. All authors commented on the manuscript.

Notes

The authors declare no competing financial interest.

ACKNOWLEDGMENTS

We acknowledge helpful discussions with Justin Song. P.G. would like to acknowledge fruitful discussions with Jaron T. Krogel and Yubo "Paul" Yang. B.M.H. was supported by the Department of Energy under the Early Career award program (#DE-SC0018115) for design of the experiments and writing of the manuscript. F.L. and D.W. were supported by the NSF DMR-1809145 for the STM measurements. The authors gratefully acknowledge NSF DMR-1626099 for acquisition of the STM instrument. F.L. was supported by the Center for Nanophase Materials Sciences, Oak Ridge National Laboratory, which is a DOE Office of Science User Facility. F.L. acknowledges funding from the Alexander von Humboldt foundation through a Feodor Lynen postdoctoral fellowship. F.L. further acknowledges funding by the Deutsche Forschungsgemeinschaft (DFG, German Research Foundation) within the Priority Programme SPP 2244 (project no. 443416235) and the Bavarian Ministry of Economic Affairs, Regional Development and Energy within Bavaria's High-Tech Agenda Project "Bausteine für das Quantencomputing auf Basis topologischer Materialien mit experimentellen und theoretischen Ansätzen". The authors thank the Pennsylvania State University Two-Dimensional Crystal Consortium -Materials Innovation Platform (2DCC-MIP), which is

Nano Letters pubs.acs.org/NanoLett Letter

supported by NSF DMR-1539916 for supplying further 2D materials. While support for initial work by A.D.P. and P.G. was by the Oak Ridge National Laboratory's Laboratory Directed Research and Development project (Project ID 7448, PI: P.G.), work on the key final results presented in the manuscript was supported by the U.S. Department of Energy, Office of Science, Basic Energy Sciences, Materials Sciences and Engineering Division, as part of the Computational Materials Sciences Program and Center for Predictive Simulation of Functional Materials. Computations were performed on the Compute and Data Environment for Science (CADES) cluster at the Oak Ridge National Laboratory, which is supported by the Office of Science of the U.S. Department of Energy under Contract No. DE-AC05-00OR22725, at the Center for Nanophase Materials Sciences, Oak Ridge National Laboratory, which is a DOE Office of Science User Facility. Crystal growth and characterization at ORNL was supported by the US Department of Energy, Office of Science, Basic Energy Sciences, Division of Materials Sciences and Engineering.

REFERENCES

- (1) Geim, A. K.; Grigorieva, I. V. Van der Waals heterostructures. *Nature* **2013**, 499, 419–425.
- (2) Qian, X.; Liu, J.; Fu, L.; Li, J. Quantum spin Hall effect in twodimensional transition metal dichalcogenides. *Science* **2014**, *346*, 1344–1347
- (3) Fei, Z.; et al. Edge conduction in monolayer WTe₂. Nat. Phys. 2017, 13, 677.
- (4) Tang, S.; et al. Quantum spin Hall state in monolayer 1T'-WTe₂. *Nat. Phys.* **2017**, *13*, 683.
- (5) Wu, S.; et al. Observation of the quantum spin Hall effect up to 100 K in a monolayer crystal. *Science* **2018**, *359*, 76–79.
- (6) Shi, Y.; et al. Imaging quantum spin Hall edges in monolayer WTe₂. Sci. Adv. **2019**, 5, No. eaat8799.
- (7) Sajadi, E.; et al. Gate-induced superconductivity in a monolayer topological insulator. *Science* **2018**, *362*, 922.
- (8) Fatemi, V.; et al. Electrically tunable low-density superconductivity in a monolayer topological insulator. *Science* **2018**, *362*, 926
- (9) Muechler, L.; Alexandradinata, A.; Neupert, T.; Car, R. Topological nonsymmorphic metals from band inversion. *Phys. Rev.* X 2016, 6, 041069.
- (10) Fei, Z.; et al. Ferroelectric switching of a two-dimensional metal. *Nature* **2018**, *560*, 336–339.
- (11) Li, P.; et al. Evidence for topological type-II Weyl semimetal WTe₂. *Nat. Commun.* **2017**, *8*, 2150.
- (12) Choi, Y.-B.; et al. Evidence of higher-order topology in multilayer WTe₂ from Josephson coupling through anisotropic hinge states. *Nat. Mater.* **2020**, *19*, 974–979.
- (13) Lüpke, F.; et al. Proximity-induced superconducting gap in the quantum spin Hall edge state of monolayer WTe₂. *Nat. Phys.* **2020**, *16*, 526–530.
- (14) Cao, Y.; et al. Correlated insulator behaviour at half-filling in magic-angle graphene superlattices. *Nature* **2018**, *556*, 80–84.
- (15) Cao, Y.; et al. Unconventional superconductivity in magic-angle graphene superlattices. *Nature* **2018**, *556*, 43–50.
- (16) Wang, L.; et al. Correlated electronic phases in twisted bilayer transition metal dichalcogenides. *Nat. Mater.* **2020**, *19*, 861–866.
- (17) Yankowitz, M.; et al. Tuning superconductivity in twisted bilayer graphene. *Science* **2019**, *363*, 1059–1064.
- (18) Lu, X.; et al. Superconductors, orbital magnets and correlated states in magic-angle bilayer graphene. *Nature* **2019**, *574*, 653–657.
- (19) Wu, F.; Lovorn, T.; Tutuc, E.; Martin, I.; MacDonald, A. H. Topological insulators in twisted transition metal dichalcogenide homobilayers. *Phys. Rev. Lett.* **2019**, *122*, 086402.

- (20) Pan, Y.; et al. Quantum-confined electronic states arising from the moiré pattern of MoS₂-WSe₂ heterobilayers. *Nano Lett.* **2018**, *18*, 1849–1855.
- (21) Serlin, M.; et al. Intrinsic quantized anomalous Hall effect in a moiré heterostructure. *Science* **2020**, *367*, 900–903.
- (22) Waters, D.; et al. Flat bands and mechanical deformation effects in the moiré superlattice of MoS₂-WSe₂ heterobilayers. *ACS Nano* **2020**, *14*, 7564–7573.
- (23) Kane, C. L.; Mele, E. J. Quantum spin hall effect in graphene. *Phys. Rev. Lett.* **2005**, 95, 226801.
- (24) Jia, Z.-Y.; et al. Direct visualization of a two-dimensional topological insulator in the single-layer 1T'-WTe₂. *Phys. Rev. B* **2017**, 96, 041108.
- (25) Arora, A.; Shi, L.-k.; Song, J. C. W. Cooperative orbital moments and edge magnetoresistance in monolayer Wte₂. *Phys. Rev. B* **2020**, *102*, 161402.
- (26) Zhao, W.; et al. Determination of the Spin Axis in Quantum Spin Hall Insulator Candidate Monolayer WTe₂. *Phys. Rev. X* **2021**, *11*, 041034.
- (27) Peng, L.; et al. Observation of topological states residing at step edges of WTe₂. *Nat. Commun.* **2017**, *8*, 659.
- (28) Wang, P.; et al. One-dimensional luttinger liquids in a two-dimensional moiré lattice. *Nature* **2022**, *605*, 57–62.

□ Recommended by ACS

Robust Quantum Anomalous Hall States in Monolayer and Few-Layer TiTe

Xiaoyu Xuan, Wanlin Guo, et al.

JULY 01, 2022

NANO LETTERS

READ 🗹

Mechanically Tunable Spontaneous Vertical Charge Redistribution in Few-Layer WTe₂

Zeyuan Ni, Satoshi Watanabe, et al.

DECEMBER 26, 2019

THE JOURNAL OF PHYSICAL CHEMISTRY C

READ 🗹

Enhanced Magnetoresistance of Doped WTe $_{\!2}$ Single Crystals

Erh-Chen Lin, Yi-Hsien Lee, et al.

AUGUST 30, 2022

ACS APPLIED ELECTRONIC MATERIALS

READ 🗹

Rashba Effect and Raman Spectra of ${\rm Tl_2O/PtS_2}$ Heterostructure

Shahid Sattar and J. Andreas Larsson

JANUARY 26, 2021

ACS OMEGA

READ 🗹

Get More Suggestions >